Sampling Error Study for Rainfall Estimate by Satellite Using a Stochastic Model

KYUNG-SUP SHIN AND GERALD R. NORTH

Climate System Research Program, College of Geosciences, Texas A&M University, College Station, Texas

(Manuscript received 30 October 1987, in final form 4 April 1988)

ABSTRACT

A parameter study of satellite orbits was performed to estimate sampling errors of area-time averaged rain rate due to temporal sampling by satellites. The sampling characteristics were investigated by accounting for varying visiting intervals and varying fractions of averaging area on each visit as a function of the latitude of the grid box for a range of satellite orbital parameters. The sampling errors were estimated by a simple model based on the first-order Markov process of the time series of area averaged rain rates.

For a satellite of nominal TRMM orbit (30° inclination and 300 km altitude) carrying an ideal scanning microwave radiometer for direct precipitation measurements, sampling error would be about 8 to 12% of estimated monthly mean rain rates over a grid box of 5° × 5°. The effect of uneven sampling intervals with latitude tend to be offset by increasing sampling areas with latitude, therefore, the latitude dependence of sampling error was not important. Nomograms for sampling errors are presented for a range of orbital parameters centered at nominal TRMM orbit. An observation system based upon the low inclination satellite combined with a sunsynchronous satellite simultaneously would be especially promising for precipitation measurements from space. Sampling errors well below 10% can be achieved for this idealized system case for the monthly rain rate estimates for 5° × 5° boxes.

1. Introduction

The rate of latent heat release is recorded in the area-time averages of rain rates. Since there is a large interannual variability of 30 day averages of rain rate even over large areas, there is reason to believe that having a dataset of this type would be very useful for testing the realism of climate models and their ability to simulate and predict climate on the seasonal time scale. Of particular interest is the rain rate over the oceans. The only means of providing a global scale dataset over the oceans is by means of space borne sensors.

Presently our only method of estimating rain rate over these areas is indirect inference from infrared cloud top temperature (Arkin 1979) from geostationary satellite. But the estimating technique is based upon a purely empirical procedure with fitted regression coefficients possibly specific to the area and season of calibration. The accuracy of this method is largely unknown and although it has proved to be very useful it must be regarded as an index until ways are found to extend the calibration over the global tropics.

The Tropical Rainfall Measuring Mission (TRMM; for more detail see the workshop report edited by Thiele 1987; also Wilheit 1986, and Simpson et al. 1988) proposes to measure precipitation directly from space throughout the tropics. The main goal of the mission is to produce a monthly mean time series of average rain rate over 5° × 5° boxes in the tropics. The mission satellite is expected to carry a multichannel scanning microwave radiometer together with an active microwave sensor and a visible/infrared sensor. The methods of inferring rain rate by microwave radiometry have been summarized by Barrett and Martin (1981). It is expected that the combination of these sensors can overcome many of the previous limitations of remote sensing of precipitation from space.

A unique feature associated with the TRMM is that the satellite will be flown at a low altitude and low inclination orbit (nominally 300 km and 30°). Due to the high spatial variability of precipitation, a small field-of-view (FOV) with respect to the scale of rain field is necessary to reduce the error due to the beam-filling problem. The beam-filling problem results from the nonhomogeneous distribution of rain rates inside a FOV and the nonlinear relationship between the rain rates and the radiant intensity. A low altitude orbit provides a small FOV for the purpose of rainfall observation from satellite without the necessity of a large expensive antenna system. Due to the expected diurnal cycle of precipitation, measurements from sun-synchronous orbit (SSO) satellites would lead to a bias in the estimation of monthly rainfall because they revisit at fixed local times at a given location. For the low

Corresponding author address: Dr. Kyung-Sup Shin, Climate System Research Program, College of Geosciences, Texas A&M, College Station, Texas 77843.

inclination orbit (LIO) satellite, which is not a SSO satellite, the observing interval at an area differs slightly from 12 h depending on the orbit parameters; therefore, it will observe precipitation through the diurnal cycle over a few weeks.

If space–time averages of a climate parameter are considered, satellite observations inherently introduce an error, called sampling error, due to temporal gaps in the observations induced by the orbit. If, on the one hand, the changing time scale of the parameter is long compared to the observing interval by satellite, such as for ice cover or ozone concentration in the stratosphere, the sampling error by satellite observation is not a problem. On the other hand, rainfall estimation from LIO satellites may be dominated by sampling errors because of the high variability of rain fields in both space and time. The objective of this study is to estimate the sampling error of area-time averaged rain rate due to discrete observations from an LIO satellite for a range of orbital parameters.

Laughlin (1981) was the first to report a study of sampling errors for precipitation estimates from satellites based upon a stochastic model. He examined the time series of area averaged rain rates and noted that the lagged autocorrelation functions were reasonably close to exponentional from the GATE [GARP Atlantic Tropical Experiment; GARP (Global Atmospheric Research Programme)] rainfall data (Hudlow and Patterson 1979). His results show that for 12 h repeated observations for flush visits (observe entire averaging area at each visit), the sampling errors for monthly rain rate estimate over 2.5° × 2.5° grid box (GATE area) were about 8%. McConnell and North (1987) employed an ensemble of imaginary orbits flying over the GATE area and collecting direct measurements toward the space–time average. Kedem et al. (1987) used a mixed probability distribution method along with the orbit ensemble and the same GATE data. Both studies showed 8% to 10% sampling errors, which were basically the same as the Laughlin's. Bell (1987) has devised a random field model that can be tuned to have many of the statistical characteristics of GATE rainfall. The model was then used to simulate the tropical rain in both spatial and temporal domains. For flush visits, Bell found that Laughlin's Markov model is an excellent imitator of his own model for sampling error studies.

All previous sampling error studies were based on idealized sampling characteristics, for flush visits and fixed sampling intervals. In the actual case, a satellite sometimes observes only a fraction of a grid box and the sampling interval is not always uniform. This study extends Laughlin's study by accounting for more realistic sampling characteristics by the satellite observing system. The emphasis is on the nominal TRMM orbit; however, the sampling errors are estimated for a range of orbits to help in the design of similar observing systems.

2. Sampling characteristics of a satellite

a. Orbital dynamics for the sampling error study

For simplicity, we shall consider only circular orbits in this study. Therefore, the discussion will be valid only for the mean motion of elliptical orbits. According to Brooks (1977), the satellite nadir track on the earth's surface is represented by

$$\phi = \sin^{-1}[\sin i \sin((\Theta + \theta)t)] \tag{1a}$$

$$\lambda = \tan^{-1}[\cos i \tan((\Theta + \theta)t)] - (\Omega - \omega)t \tag{1b}$$

where

- ϕ, λ latitude and longitude,
- i inclination of satellite orbit,
- Θ perturbed mean angular velocity of the satellite on its orbital plane,
- θ angular velocity of precession on its orbital plane due to earth's oblateness,
- ω angular velocity of precession on the equatorial plane due to earth's oblateness,
- Ω earth's angular velocity on the equatorial plane,
- t time, and
- h the satellite altitude.

Since Θ, θ, and ω are functions of i and h only, they will be constants for given orbital parameters. The schematic of definitions of the orbital angles and their relationships are presented in appendix A (see Brooks' analysis for more detail).

Let $\Theta + \theta = \alpha$ and $\Omega - \omega = \beta$, then from (1a) and (1b), it is easily shown that

$$t = \frac{1}{\alpha}\left[2\pi n + \sin^{-1}\left(\frac{\sin\phi}{\sin i}\right)\right]$$

$$= n\tau_n + \frac{1}{\alpha}\sin^{-1}\left(\frac{\sin\phi}{\sin i}\right), \tag{2}$$

and

$$\lambda = -\frac{\beta}{\alpha}\left[2\pi n + \sin^{-1}\left(\frac{\sin\phi}{\sin i}\right)\right] + \tan^{-1}\left[\cos i \tan\left(\sin^{-1}\left(\frac{\sin\phi}{\sin i}\right)\right)\right] \tag{3}$$

where n (integer) is the number of rotations and τ_n is the nodal period of the satellite for the given orbit. Then, (2) gives the time at which the satellite crosses latitude ϕ in rotation n, and (3) gives the longitude when satellite passes latitude ϕ. Since '$\sin^{-1}(x)$' is a double valued function, it is better to distinguish the ascending and descending nodes. Then for the ascending node,

$$t_a = \frac{1}{\alpha}\left[2\pi n + \sin^{-1}\left(\frac{\sin\phi}{\sin i}\right)\right], \tag{2a}$$

while for the descending node,

$$t_d = \frac{1}{\alpha}\left[2\pi n + \pi - \sin^{-1}\left(\frac{\sin\phi}{\sin i}\right)\right]. \quad (2b)$$

Similarly,

$$\lambda_a = -\frac{\beta}{\alpha}\left[2\pi n + \sin^{-1}\left(\frac{\sin\phi}{\sin i}\right)\right] + \tan^{-1}\left[\cos i \tan\left(\sin^{-1}\left(\frac{\sin\phi}{\sin i}\right)\right)\right] \quad (3a)$$

$$\lambda_d = -\frac{\beta}{\alpha}\left[2\pi n + \pi - \sin^{-1}\left(\frac{\sin\phi}{\sin i}\right)\right] + \pi - \tan^{-1}\left[\cos i \tan\left(\sin^{-1}\left(\frac{\sin\phi}{\sin i}\right)\right)\right] \quad (3b)$$

where $-\frac{\pi}{2} \leqslant \sin^{-1}\left(\frac{\sin\phi}{\sin i}\right) \leqslant \frac{\pi}{2}$. From (2a), (2b), (3a), and (3b),

$$t_{a_{n+1}} - t_{a_n} = t_{d_{n+1}} - t_{d_n} = \frac{2\pi}{\alpha} = \tau_n$$

$$\lambda_{a_{n+1}} - \lambda_{a_n} = \lambda_{d_{n+1}} - \lambda_{d_n} = -\frac{\beta}{\alpha}(2\pi) = -\beta\tau_n$$

and

$$t_{d_n} - t_{a_n} = \frac{1}{\alpha}\left[\pi - 2\sin^{-1}\left(\frac{\sin\phi}{\sin i}\right)\right]$$

$$\lambda_{d_n} - \lambda_{a_n} = -\frac{\beta}{\alpha}\left[\pi - 2\sin^{-1}\left(\frac{\sin\phi}{\sin i}\right)\right] + \pi - 2\tan^{-1}\left[\cos i \tan\left(\sin^{-1}\left(\frac{\sin\phi}{\sin i}\right)\right)\right].$$

Therefore, the ascending and descending nodes can be treated as separate sequences which differ in initial phase depending on ϕ.

The following two expressions will be useful for later purposes;

$$\Delta t = \frac{2\pi}{\beta} = f(i, h)$$

$$\Delta t_d = \frac{1}{\beta}\left[\pi - 2\sin^{-1}\left(\frac{\sin\phi}{\sin i}\right)\right] = f(i, h, \phi)$$

where Δt is the approximate time from one observation by an ascending (descending) node to the next observation by an ascending (descending) node over a particular spot on the earth. Likewise, Δt_d is the approximate time from one observation by an ascending (descending) node to that by a descending (ascending) node. For the SSO, $\Delta t = 1$ *day*. If the orbital parameters do not satisfy the condition $\Delta t = 1$ *day*, e.g., for an LIO, the orbital plane will precess either eastward ($\Delta t > 1$ *day*) or westward ($\Delta t < 1$ *day*) with respect to the earth. In other words, the orbital plane of the LIO satellites would visit the same area at intervals either longer or shorter than a day depending on the orbital parameters. Therefore they will observe a given area through the diurnal cycle over a few weeks.

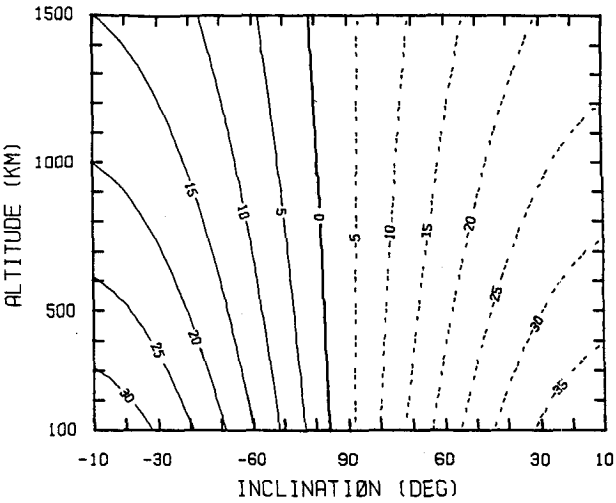

FIG. 1. The visiting time difference from that of a sun-synchronous orbit in minutes. The negative values are represented by dashed lines. The positive inclination indicate prograde orbit and negative for retrograde orbit.

The deviation of Δt from 1 *day* for various orbits is summarized in Fig. 1. In this figure we plot the difference (in minutes) between the visiting interval of the given LIO and that of a SSO. The zero line indicates the SSOs. The figure encompasses all practical satellite orbits and hence demonstrates that the visiting interval by an ascending (descending) node will be limited within 30 min from 24 h. For the proposed TRMM orbit, the visiting time is about 23 h and 27 min. Therefore, in about 44 days, the satellite will return its ascending node to the original position.

For the sampling error study, we consider a certain grid box ($L° \times L°$) on the earth centered at ϕ_0 and λ_0. Figure 2 illustrates the schematic diagram used to investigate the sampling characteristics of satellite observations. If an ascending node of a satellite nadir track crosses between λ_l and λ_r (effective width, $\Delta\lambda_e$) at latitude ϕ_0, the satellite observes some fraction of the grid box, depending on the distance of the nadir track from the center of the grid box. The effective width will be

$$\Delta\lambda_e = \lambda_r - \lambda_l = 2(\Delta\lambda_1 + \Delta\lambda_2 + \Delta\lambda_3).$$

Note that this relation is also applicable to the descending node because of symmetry. It is easily shown that

$$\Delta\lambda_1 = \frac{1}{2}L,$$

$$\Delta\lambda_2 = \frac{1}{2}L\left(\left|\frac{d\phi}{d\lambda}\right|\right)^{-1},$$

$$\Delta\lambda_3 = \delta_1/\cos\phi_0,$$

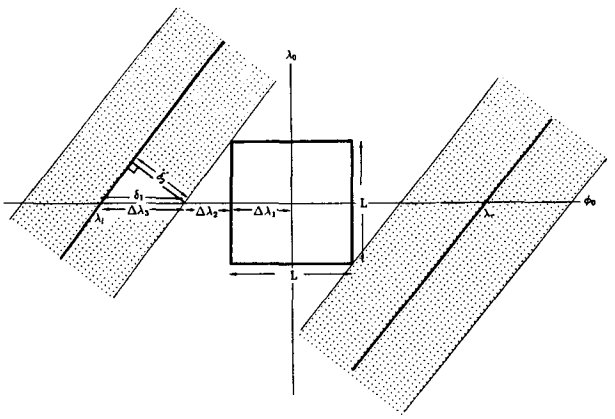

FIG. 2. The schematic diagram to calculate effective width for the given $L° \times L°$ grid box located at (ϕ_0, λ_0). The dotted areas indicate the satellite scan width.

where $\left(\frac{d\phi}{d\lambda}\right)$ is the slope of the nadir track with respect to the earth coordinate system, and δ_1 (and δ_2) are angles measured from the center of the earth. Again, from the law of sines on a spherical triangle,

$$\frac{\sin\delta_1}{\sin\left(\frac{\pi}{2}\right)} = \frac{\sin\delta_2}{\sin\left[\tan^{-1}\left(\left|\frac{d\phi}{d\lambda}\right|\right)_{\phi_0}\right]},$$

and from the law of sines on a plane triangle,

$$\delta_2 = \sin^{-1}\left(\frac{a+h}{a}\sin\gamma\right) - \gamma,$$

where γ is the maximum angle of observation perpendicular to the nadir track by an instrument on the satellite, δ_2 is the corresponding angle from the center of the earth, a the radius of the earth, h the satellite altitude. Therefore,

$$\Delta\lambda_3 = \sin^{-1}\left\{\frac{\sin\left[\sin^{-1}\left(\frac{a+h}{a}\sin\gamma\right) - \gamma\right]}{\sin\left[\tan^{-1}\left(\left|\frac{d\phi}{d\lambda}\right|\right)\right]}\right\} \Big/ \cos\phi_0.$$

Finally,

$$\Delta\lambda_e(\phi_0) = L\left[1 + \left(\left|\frac{d\phi}{d\lambda}\right|\right)^{-1}_{\phi_0}\right] + 2\sin^{-1}\left\{\frac{\sin\left[\sin^{-1}\left(\frac{a+h}{a}\sin\gamma\right) - \gamma\right]}{\sin\left[\tan^{-1}\left(\left|\frac{d\phi}{d\lambda}\right|\right)_{\phi_0}\right]}\right\} \Big/ \cos\phi_0. \tag{4}$$

From (3), the slope of the satellite ground track, $\left(\frac{d\phi}{d\lambda}\right)$, can be calculated from

$$\left(\frac{d\phi}{d\lambda}\right) = \frac{\left\{(\cos^2 i - 1)\sin^2\left[\sin^{-1}\left(\frac{\sin\phi}{\sin i}\right)\right] + 1\right\}\sin i\sqrt{1 - \left(\frac{\sin\phi}{\sin i}\right)^2}}{\cos\phi\left\{\cos i - \frac{\beta}{\alpha}\left\{(\cos^2 i - 1)\sin^2\left[\sin^{-1}\left(\frac{\sin\phi}{\sin i}\right)\right] + 1\right\}\right\}}.$$

Since the slope is a function only of orbital parameters (i, h), for a given satellite orbit, the effective width depends on a size of area (L), and the viewing angle of instrument (γ). For the given grid box size and swath width, the visiting time sequences can be calculated by using (2), (3), and (4). The fractional coverage can also be calculated by the difference of longitude from the center on each visit.

b. *Sampling characteristics of satellite observations*

We restrict our attention in this study to a $5° \times 5°$ grid box on the earth ($L = 5°$), observed by an ideal passive microwave device whose beam is scanned across track $\pm 50°$ ($\gamma = 50°$). It is interesting to see the ratio of effective width to the longitude separation for one nodal period $(\Delta\lambda_e/\beta\tau_n)$. This dimensionless number gives a measure of overlapping of observations on a given grid box during consecutive rotations. It will be referred to as Normalized Effective Width (NEW) hereafter. If the NEW is less than unity, it is possible to miss observations of a given grid box on a given day. If the value is between one and two, there must be at least one observation of some fraction of the given grid box in a day by an ascending (descending) node. Moreover, there is a chance of two observations by two consecutive ascending (descending) nodes in a day. For a value greater than two, there must be at least two observations by the two consecutive ascending (descending) nodes, and so on.

The NEW forms a three dimensional parameter space (for altitude, inclination, and latitude) for the given grid box and observing system. Figure 3 shows the NEW with orbit parameters at the equator for γ

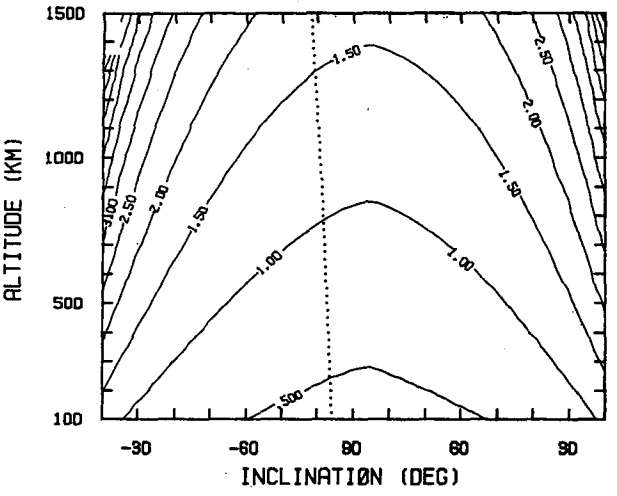

FIG. 3. The normalized effective width with respect to orbit parameters at the equator, for the 5° × 5° grid box and the ±50° swath. The dotted line indicates the sunsynchronous orbits.

= 50° and L = 5°. For fixed inclination, the NEW increases with increasing altitude because viewing area ($\Delta\lambda_3$ in Fig. 2) increases more rapidly than the longitude separation in one rotation. For fixed altitude, the NEW decreases with steepening inclination because $\Delta\lambda_2$ and $\Delta\lambda_3$ decrease. Note that Fig. 3 is not symmetric due to the earth rotation as Fig. 1 is.

Figure 4 illustrates an example of change of the NEW with respect to latitude and size of grid box for the nominal TRMM orbit. As L increases, the NEW obviously increases. The NEW also increases with increasing latitude due to the flattening slope of the nadir track such that the longitudinal sweep increases. Therefore, two or more consecutive rotations can observe some fraction of the given grid box at the near turning latitudes. In other words, the sampling area increases with increasing latitude.

Figure 5 illustrates the visiting sequences and changing fractional coverage through a month for some selected orbits at the equator. For each orbit the ordinate indicates the day of month and the abscissa is the local time of the day. The graphs in the last column are the examples for the sun-synchronous orbits for different altitudes. In each graph, the complete squares indicate that satellite observes the entire 5° × 5° grid box (flush visit) at the time and day specified by the coordinates. Any triangles or trapezoids illustrate partial visits by that fraction out of the entire grid box. There are basically two observations a day by ascending and descending nodes, and the sampling intervals between the ascending and descending nodes (Δt_d) are equal at the equator. The slope of observations by each node represents the visiting time difference from 24 h as presented in Fig. 1. All the sampling sequences can be explained by the corresponding value of the NEW in Fig. 3. Note that there may be no observation on a certain day if the NEW is less than unity. This is also true for some SSOs (e.g., 500 km altitude). The SSO with 1000 km altitude comes close to the flush visit. Note that if an observation covers only a fraction of grid box, then the next visit covers the other fraction.

For the given satellite orbit, the fractional coverage is also a function of latitude as shown in Fig. 4. Moreover, the sampling intervals are different because the times between the ascending and descending nodes become more unequal with increasing latitude. Figure 6 shows an example of the different sampling characteristics with respect to latitude for the proposed TRMM orbit. With increasing latitude, the sampling interval between the ascending to descending node gets longer while the sampling interval between the descending to ascending node gets shorter. At 30°, the two nodes merge together (one observation in a day, basically). However, the observing area increases with increasing latitude.

As a consequence, the sampling characteristics of satellite observation depend on the orbital parameters (altitude and inclination) and latitude for the given grid size and instrument. For the sampling error study, which we will perform in the next section, the variation of fractional coverage and uneven sampling interval with latitude will be taken into account. This estimation will be helpful in understanding the performance of satellites.

3. Sampling error estimation

a. Sampling error

Laughlin (1981) proposed a formula permitting estimation of the mean square error (MSE) of the mean

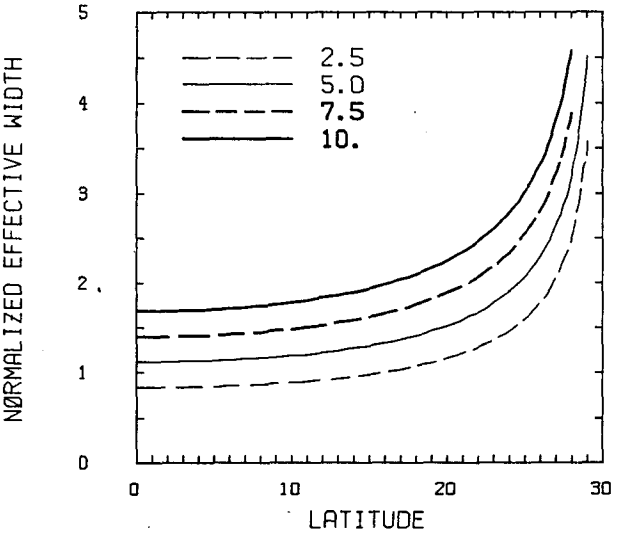

FIG. 4. The normalized effective width with respect to latitude and size of grid box for the TRMM orbit (300 km altitude and 30° inclination). Four different grid box sizes are chosen (2.5°^{2}, 5.0°^{2}, 7.5°^{2}, and 10.0°^{2}).

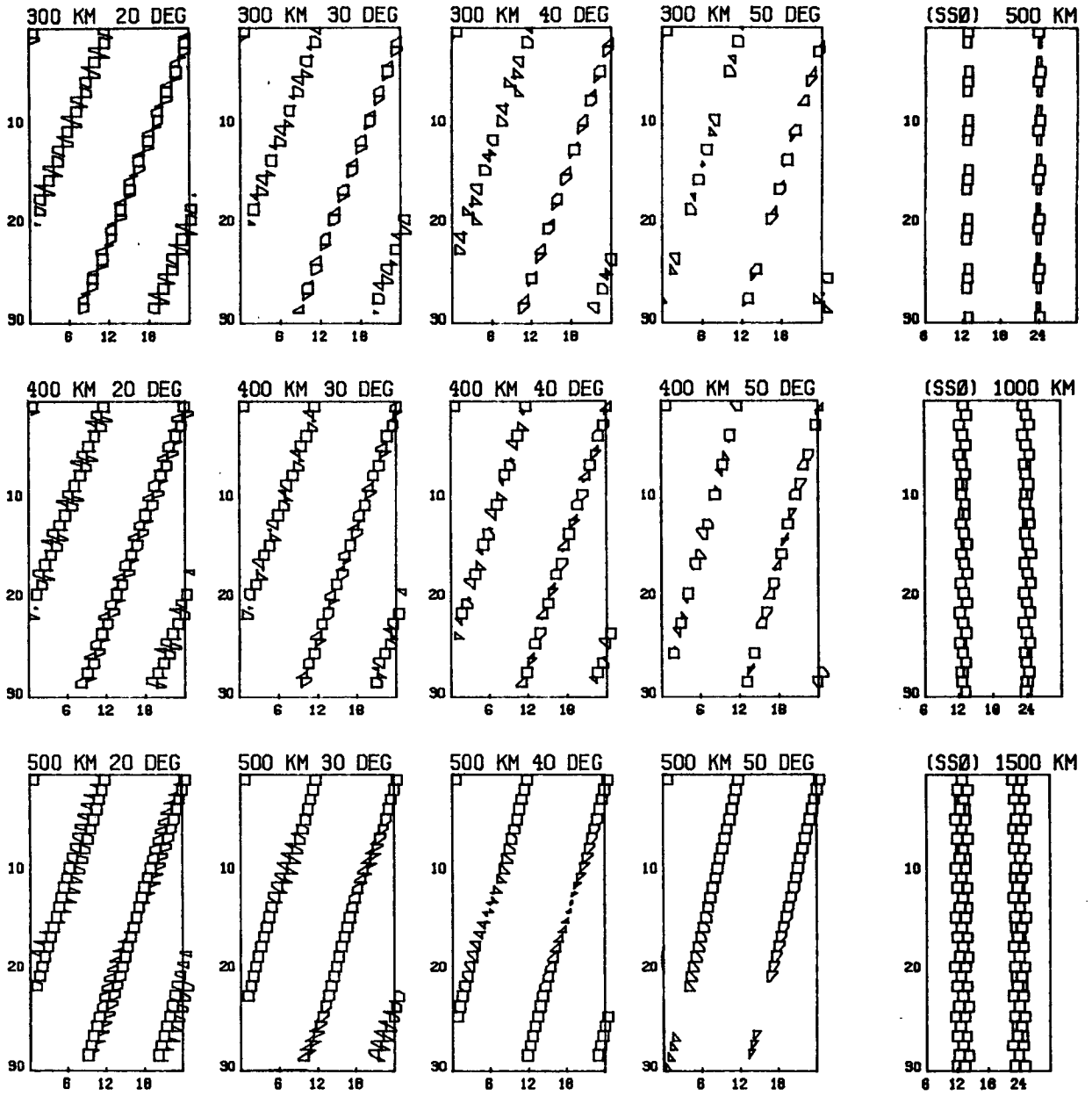

FIG. 5. The visiting sequences and fractional coverages through a month for some selected orbits at the equator. For each orbit, the ordinate indicates the day of month and the abscissa indicate local time of the day. The last column is for sunsynchronous orbits for altitudes (inclination) 500 km (97.37°), 1000 km (99.44°), and 1500 km (101.90°).

value of a random variable due to periodic sampling. His formula was then applied to estimate the sampling error for satellite observations of space–time mean rain rates. His parameters were tuned to fit data from GATE. Since his development was based on the sampling by a SSO satellite with flush visits, his approach must be modified to take into account the sampling characteristics shown in the previous section. Laughlin's development is reproduced in appendix B because his work was not published in a widely accessible form.

Let the real mean, $M(T)$, for arbitrary time interval T for a random variable $X(t)$ be

$$M(T) = \frac{1}{T}\int_0^T X(t)\mathrm{d}t.$$

The $X(t)$ is an area averaged rain rate, $A^{-1}\int_A R(\mathbf{r}, t)d\mathbf{r}$, in this study. In practice, a continuous record of $X(t)$ is seldom available. If we assume spatially homogeneous rainfall statistics, an estimate of $M(T)$ by satellite observation would be

$$\hat{M}(T) = \sum_{i=0}^{N-1} f_i X_i(i\Delta t) / \sum_{i=0}^{N-1} f_i,$$

where $T = N\Delta t$ and $X_i(i\Delta t)$ would be a subarea averaged rain rate for the fraction of f_i,

$$X_i(i\Delta t) = A_i^{-1} \int_{A_i} R(\mathbf{r}, t_i)\mathrm{d}\mathbf{r} \quad \text{with} \quad A_i = f_i A.$$

Then the MSE can be estimated by $E[(\hat{M}(T) - M(T))^2]$, where 'E' denotes the expected value. As a first approximation, $X_i(i\Delta t)$ is substituted for by $X(i\Delta t)$, i.e.,

$$\hat{M}(T) = \sum_{i=0}^{N-1} f_i X(i\Delta t) / \sum_{i=0}^{N-1} f_i.$$

Since $A_i \leq A$, $\mathrm{Var}(X_i(i\Delta t)) \geq \mathrm{Var}(X(i\Delta t))$, and the area averaged rainrate over small areas has a shorter correlation time and will be less correlated with previous and subsequent rainfall; these factors may tend to decrease MSE. However, the variances of area averaged rain rates tend to decrease as the $-1/3$ power of averaging area (North 1987), and the weight is proportionally applied to the fractional coverage. Therefore we do not expect a significant change in MSE by the substitution, although our substitution does give a lower limit of MSE. (We thank T. L. Bell for his comment on this point by personal communication.) An approach which avoids the approximation used here is that of Bell (1987). He constructs a random field which has most of the statistical characteristics of GATE data. Using the simulated rain field, he can fly over with an ensemble of satellites using all the features of a simulated observing system. This research is presently in progress. The advantage of the present approach is simplicity and economy.

Although the sampling interval between ascending (descending) nodes are not always the same as seen in Figs. 5 and 6, they would be different within only one nodal period if we assign no weight ($f_i = 0$) in the case of no observation. Then '$2\pi/\beta$' (Δt) would be a good parameter for representing average sampling interval between ascending (descending) nodes. Hence they can be treated as two individual sampling series which have the initial sampling time difference of Δt_d depending on the latitude. For example, Δt_d is the half of Δt at the equator and zero at 30° when the satellite inclination is 30°. Then, the estimated mean rain rate, $\hat{M}(T)$, from satellite observation can be written

$$\hat{M}(T) = \frac{1}{\sum_{i=0}^{N-1} a_i + \sum_{j=0}^{N-1} b_j} \Big[\sum_{i=0}^{N-1} a_i X(t + i\Delta t) + \sum_{j=0}^{N-1} b_j X(t + \Delta t_d + j\Delta t) \Big],$$

where a_i and b_j are the fractional coverage of each visit by the ascending and descending nodes, respectively. No attempt was made in this study to optimally weight the visits using prior information about correlations across a box (frequent visits to only a small part of the grid box may be worth more than occasional large area visits because of distance correlations) although this is clearly a subject for future study.

By following the calculation procedure suggested by Laughlin (see appendix B), the MSE can be expressed by

$$\begin{aligned}\sigma_e^2 = {} & \frac{2}{T}\int_0^T \left(1 - \frac{\tau}{T}\right) R(\tau)\mathrm{d}\tau + \frac{1}{(\sum_{i=0}^{N-1} a_i + \sum_{j=0}^{N-1} b_j)^2} \\ & \times \Big\{ R(0) \sum_{k=0}^{N-1} (a_k^2 + b_k^2) + 2R(\Delta t_d) \sum_{k=0}^{N-1} (a_k b_k) \\ & + 2 \sum_{k=1}^{N-1} R(k\Delta t) \sum_{j=0}^{N-(k+1)} (a_j a_{j+k} + b_j b_{j+k}) \\ & + 2 \sum_{k=1}^{N-1} R(k\Delta t + \Delta t_d) \sum_{j=0}^{N-(k+1)} (a_j b_{j+k}) \\ & + 2 \sum_{k=1}^{N-1} R(k\Delta t - \Delta t_d) \sum_{j=0}^{N-(k+1)} (a_{j+k} b_j) \Big\} \\ & - \frac{2}{T(\sum_{i=0}^{N-1} a_i + \sum_{j=0}^{N-1} b_j)} \Big\{ \sum_{k=0}^{N-1} a_k \int_0^T R(\tau - k\Delta t)\mathrm{d}\tau \\ & + \sum_{l=0}^{N-1} b_l \int_0^T R(\tau - l\Delta t - \Delta t_d)\mathrm{d}\tau \Big\}. \quad (5)\end{aligned}$$

Here τ represents the time lag and $R(\tau)$ is the autocovariance function at the time lag τ. Using the GATE rainfall data during the Phase 1 and 2, Laughlin (1981) calculated the autocovariance functions of the area-averaged rainfall, and fitted them to a first order Markov process with good agreements, that is, $R(\tau) = Be^{-|\tau|/\tau_0}$. By substituting this into (5),

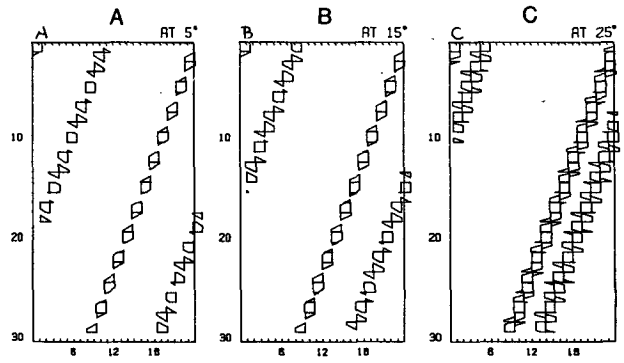

FIG. 6. The visiting sequences and fractional coverages through a month for the TRMM orbit (300 km altitude and 30° inclination) for different latitudes (A: at 5°, B: at 15°, C: at 25°).

$$\sigma_e^2 = B\Bigg[\frac{2}{T}\tau_0 + \frac{2}{T^2}\tau_0^2(e^{-T/\tau_0} - 1)$$
$$+ \frac{1}{(\sum_{i=0}^{N-1} a_i + \sum_{j=0}^{N-1} b_j)^2}\{\sum_{k=0}^{N-1}(a_k^2 + b_k^2)$$
$$+ 2e^{-\Delta t_d/\tau_0} \times \sum_{k=0}^{N-1}(a_k b_k)$$
$$+ 2\sum_{k=1}^{N-1} e^{-k\Delta t/\tau_0} \times \sum_{j=0}^{N-(k+1)}(a_j a_{j+k} + b_j b_{j+k})$$
$$+ 2\sum_{k=1}^{N-1} e^{-(k\Delta t+\Delta t_d)/\tau_0} \times \sum_{j=0}^{N-(k+1)}(a_j b_{j+k})$$
$$+ 2\sum_{k=1}^{N-1} e^{-(k\Delta t-\Delta t_d)/\tau_0} \times \sum_{j=0}^{N-(k+1)}(a_{j+k} b_j)\}$$
$$- \frac{2\tau_0}{T(\sum_{i=0}^{N-1} a_i + \sum_{j=0}^{N-1} b_j)} \times$$
$$\{\sum_{k=0}^{N-1} a_k(2 - e^{-k\Delta t/\tau_0} - e^{-(T-k\Delta t)/\tau_0})$$
$$+ \sum_{l=0}^{N-1} b_l(2 - e^{-(k\Delta t+\Delta t_d)/\tau_0} - e^{-(T-k\Delta t-\Delta t_d)/\tau_0})\}\Bigg]. \quad (6)$$

Note that for the special case when $\Delta t_d = \Delta t/2 = 12$ h and flush visit ($a_i = b_j = 1$), (5) and (6) are identical to the (B8) and (B9), respectively in appendix B. Customarily, sampling error is expressed by standard error (σ_e) in percent of mean, that is, $\sigma_e/\bar{X}$ where $\bar{X}$ is the mean rain rate. All but $\sqrt{B}/\bar{X}$ (coefficient of variation; CV) and τ_0 can be determined by the given orbit parameters in (6).

Laughlin's study indicates that τ_0 depends on the averaging area. Bell (1987) showed the relationship between the τ_0 and the averaging area ($A = L^2$) from the range of 4×4 km^2 to 280×280 km^2 to be $\tau_0(L) = CL^{2/3}$ using the GATE I data, where $C = 0.24$ when τ_0 is expressed in units of hours and L in km. Therefore, by simple extrapolation, it will be about 16 h for the $5° \times 5°$ area. However, to be conservative, *we have chosen τ_0 to be 12 h in this study.* The value of CV for the $5° \times 5°$ area is still in question. Figure 7 shows the relationship of CV with respect to the size of grid box using Laughlin's data during the Phase 1 and 2 in GATE. We do not attempt to extrapolate up to the 550 *km* size; however, it is believed that the value would be between 1.5 to 1.0 for a grid size of about 550 *km*. We have chosen the value of 1.0 in this study since it is in agreement with the more detailed rainfield model suggested by Bell (1987 and private communication).

When two or more consecutive ascending or descending nodes observe some fractions in the given grid box, they were summed to represent a single value of fractional coverage, and if the sum is larger than one, it is assigned to be one. This is based on the assumption that rain fields do not significantly differ in one nodal period (typically 90 to 100 min). The sampling errors for the $5° \times 5°$ grid box by the *perfect* microwave radiometer are estimated for various satellite orbits within the tropical area. The results are presented in the following section.

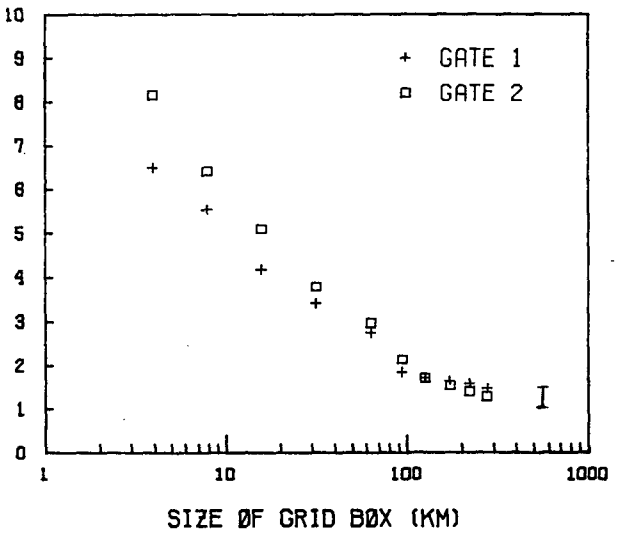

FIG. 7. The coefficient of variation ($\sqrt{B}/\bar{X}$) of area-averaged rain rates with respect to the size of grid box in GATE 1 and 2. Vertical bar indicates the values between 1.0 and 1.5 at 550 km.

It is emphasized that the method used is based on the fact that the time series of a large area averaged rain rates in GATE are reasonably close to the first order Markov, which was found by Laughlin using the actual GATE data. Therefore Laughlin concluded that any diurnal variation in GATE area was an insignificant factor. However, an independent study by Albright et al. (1981) showed evidence of existance of a substantial diurnal cycle in the GATE. Later studies after GATE have also shown (Reed and Jaffe 1981) that the diurnal cycle of GATE 1 and 3 are in fact the characteristic ones of the region in summer. The GATE area diurnal variation is strongly dominated by a single harmonic. Albright et al. (1985) present evidence that a second harmonic is often appreciable over vast regions over the Pacific. Presence of a second harmonic causes bias in the observations for a SSO satellite which visits the same grid box precisely every 12 h.

b. *Sampling errors for average rain rate estimate by satellite*

Figure 8 summarizes the sampling errors of the monthly area averaged rain rate estimate for the nominal TRMM orbit versus latitude of the grid box. The solid line is for the flush visit case as the limits of sampling errors on the given orbit, and the dashed line is for the partial visit (realistic) case. (Ignore heavy broken line at this moment. It will be referred to in the section

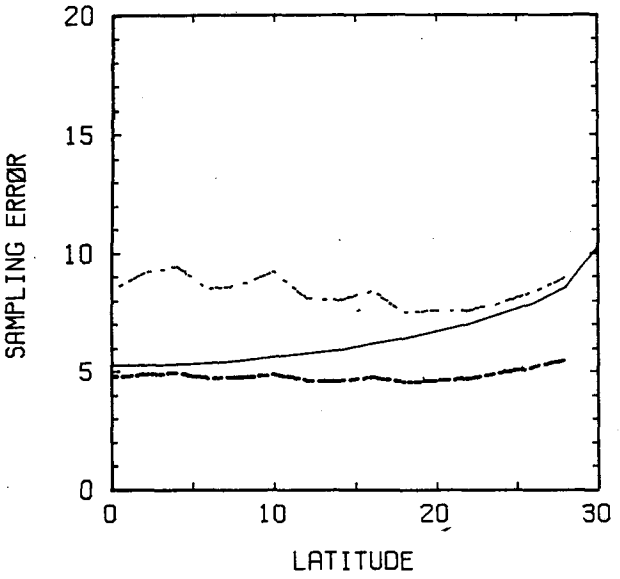

FIG. 8. Sampling error (standard deviation σ_e in percent of mean) for the monthly mean rainrate estimate with respect to latitude for the TRMM orbit. Dashed line is for the partial visit, solid line is for the flush visit. The heavy broken line indicates the sampling error for the simultaneous observation by the TRMM satellite and a sun-synchronous satellite (see section 4).

4.) For the flush visit case, sampling error increases with increasing latitude because of uneven periodic visits by ascending and descending nodes. This indicates that the effective number of independent samples decreases as sampling intervals become more asymmetrical. At 30° sampling error increases to twice that at the equator for the TRMM orbit. However, this effect is offset by the increasing sampling area with latitude when fractional coverage is considered. Therefore, the latitude dependence of the errors is negligible. The wave-like variation on the sampling error results from the periodic variation of correlation of fractional coverages between the ascending and descending nodes with respect to latitude [see Eq. (6)]. On the average, the sampling error would be about 10% for the monthly mean rainfall estimate over the 5° × 5° area for the proposed TRMM satellite observations. However, due to the uncertainties of the extrapolated values of τ_0 and CV on 5° × 5° area, estimation was performed for other possible parameter values. Table 1 summarizes the sampling errors for other extrapolated parameter values of τ_0 and CV. It ranges from 8% to 15%; however, we feel that the extremes corresponding to values of CV = 1.5 and τ_0 = 8 h are so unlikely that we favor expressing the range as 8% to 12%.

Figure 9 shows the sampling errors of monthly area averaged rain rates for various satellite orbits. To confine our discussion in the tropical region, the average value between the latitudes 20s is calculated on each orbit. Generally, sampling error decreases with increasing altitude and decreasing inclination. For the altitude higher than 1000 km, samplings are close to the flush visit, therefore, sampling errors do not vary significantly with orbits. The increasing sampling error for the low inclination at high altitude is due to the latitude effect (uneven sampling period). Note that the sampling error of the TRMM orbit is almost equivalent to that of the SSO with 700 km altitude. Even though they provide the same sampling error, the FOV of the TRMM satellite is factor of two smaller than that of the SSO satellite, therefore, the error due to the beam-filling problem would be reduced. Furthermore, the expected additional errors due to the diurnal cycle of the rainfield will be added to the SSO observation, while they tend to be canceled by the TRMM satellite observation.

TABLE 1. Sampling errors for parameter values of coefficient of variation (CV) and integral time scale (τ_0) for area-averaged rain rates for 5° × 5° area.

	CV		
τ_0 (hour)	1.0	1.25	1.5
8	10.3	12.9	15.4
12	8.4	10.5	12.6
16	7.6	9.5	11.5

4. Sampling error for multi-satellite observations

It is very interesting to estimate the sampling error for the case of multi-satellite observation for future planning. In this section we will consider two special cases, observations by two simultaneous SSO satellites and by the TRMM satellite and one SSO satellite. In any case, it is assumed that precipitation is observed by the same microwave sensors, and they are perfect

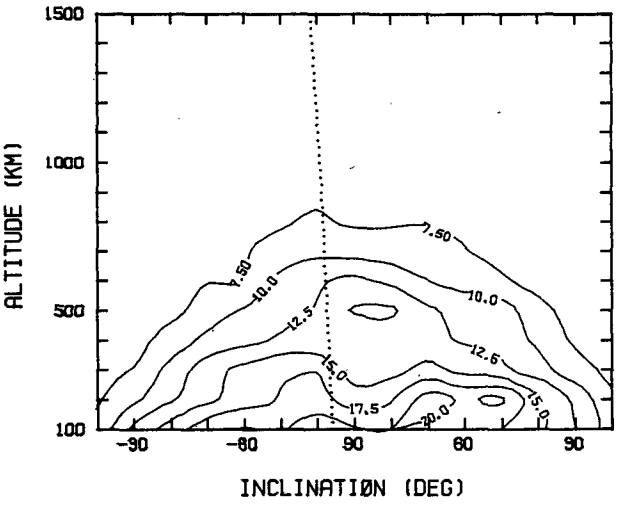

FIG. 9. Average sampling error for the monthly mean rainrate estimates between latitudes 20° for the orbit parameters. The dotted line indicates the sunsynchronous orbits.

so that no optimal weighting scheme is required due to different measurement errors for the different spacecraft. In addition, the altitude of the SSO satellite is assumed to be high enough for the flush visit assumption on a given 5° × 5° grid box to apply.

The two SSO satellite observations can reduce observation interval shorter than 12 h depending upon their phase difference (Δt_d). If Δt_d is 6 h, four observations are available in a day on a given area with 6 h interval, for example. In this case, the estimated mean can be expressed by

$$\hat{M}_{SS}(T) = \frac{1}{2N}\left[\sum_{i=0}^{N-1} X(t + it_0) + \sum_{j=0}^{N-1} (t + \Delta t_d + jt_0)\right]$$

where t_0 is 12 h. Following the same algebra as before, the MSE for two SSO satellites observation is

$$\sigma_{SS}^2 = \frac{B}{(T/\tau_0)}\left[-2 + \frac{t_0}{2\tau_0}\frac{\{(e^{\Delta t_d/\tau_0}+1) + e^{t_0/\tau_0}(e^{-\Delta t_d/\tau_0}+1)\}}{(e^{t_0/\tau_0}-1)} + \frac{(e^{-T/\tau_0}-1)}{(T/\tau_0)}\left\{2 - \frac{t_0}{\tau_0} \times \frac{\{(e^{\Delta t_d/\tau_0}+1) + e^{t_0/\tau_0}(e^{-\Delta t_d/\tau_0}+1)\}}{(e^{t_0/\tau_0}-1)} + \frac{1}{2}\left(\frac{t_0}{\tau_0}\right)^2 \frac{e^{t_0/\tau_0}(e^{-\Delta t_d/\tau_0}+2+e^{\Delta t_d/\tau_0})}{(e^{t_0/\tau_0}-1)^2}\right\}\right]. \quad (7)$$

Note that when $\Delta t_d = 0$ or t_0, (7) is identical to (B9) for the case of one SSO satellite observation in appendix B.

Figure 10 shows the sampling error by two SSO satellites observation with different Δt_d. When Δt_d is 0 or 12 h, which is equivalent to one SSO satellite observation, the sampling error would be about 6%. However, the sampling error reduces by a factor of two when sampling intervals become even. Therefore, the sampling error can be reduced to about 3% by using two SSO satellites. The diurnal cycle in rain field would not be significant in this case because this system can average out the harmonics up to the second in the 6 h interval case. However, the large FOV due to high altitude could add large errors due to the beam-filling problem.

For the case of the TRMM satellite and one SSO satellite, the estimate of mean rain rate can be written by

$$\hat{M}_{TS}(T) = \frac{1}{W}\left[\sum_{i=0}^{N-1} a_i(t + i\Delta t) + \sum_{j=0}^{N-1} b_j(t + \Delta t_d + j\Delta t) + \sum_{k=0}^{M-1} X(t + kt_0)\right]$$

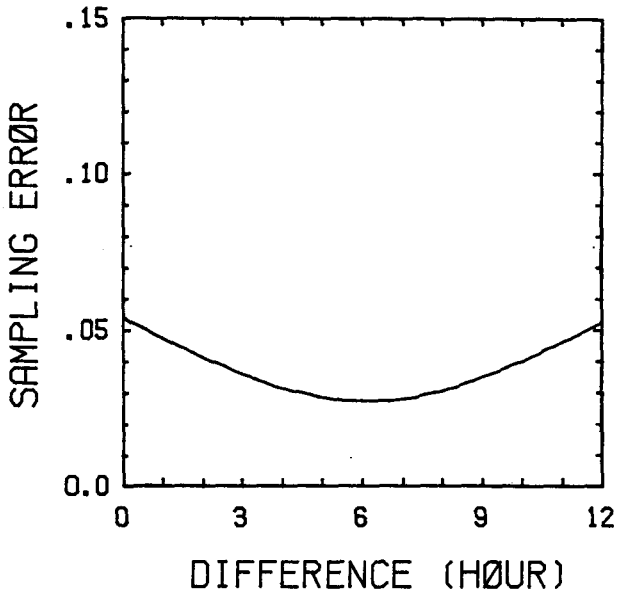

FIG. 10. Sampling error for the monthly mean rainrate estimate by two sunsynchronous satellite observation with different phase.

where $W = (\sum a_i + \sum b_j + M)$ and $Mt_0 = T$. Again same procedure will give

$$\sigma_{TS}^2 = B\left[\frac{2}{T}\tau_0 + \frac{2}{T^2}\tau_0^2(e^{-T/\tau_0}-1) + \frac{1}{W^2}\left\{\sum_{k=0}^{N-1}(a_k^2+b_k^2) + 2e^{-\Delta t_d/\tau_0}\sum_{k=0}^{N-1}(a_k b_k) + 2\sum_{k=1}^{N-1} e^{-k\Delta t/\tau_0}\sum_{j=0}^{N-(k+1)}(a_j a_{j+k} + b_j b_{j+k}) + 2\sum_{k=1}^{N-1} e^{-(k\Delta t+\Delta t_d)/\tau_0}\sum_{j=0}^{N-(k+1)}(a_j b_{j+k}) + 2\sum_{k=1}^{N-1} e^{-(k\Delta t-\Delta t_d)/\tau_0}\sum_{j=0}^{N-(k+1)}(a_{j+k} b_j) + 2\sum_{i=0}^{N-1}\sum_{k=0}^{M-1} a_i e^{-|i\Delta t-kt_0|/\tau_0} + 2\sum_{j=0}^{N-1}\sum_{k=0}^{M-1} b_j e^{-|j\Delta t+\Delta t_d-kt_0|/\tau_0}\right\} + \frac{T}{t_0}\left(1 + 2\frac{\left\{e^{\Delta t/\tau_0} - 1 + \frac{\Delta t}{T}e^{\Delta t/\tau_0}\right\}(e^{-T/\tau_0}-1)}{(e^{\Delta t/\tau_0}-1)^2}\right)\right\}$$

$$-\frac{2\tau_0}{TW}\left\{\sum_{k=0}^{N-1} a_k(2-e^{-k\Delta t/\tau_0}-e^{-(T-k\Delta t)/\tau_0})\right.$$

$$+\sum_{l=0}^{N-1} b_l(2-e^{-(k\Delta t+\Delta t_d)/\tau_0}-e^{-(T-k\Delta t-\Delta t_d)/\tau_0})$$

$$\left.+\sum_{k=0}^{M-1}(2-e^{-kt_0/\tau_0}-e^{-(T-kt_0)/\tau_0})\right\}\Bigg]. \quad (8)$$

The results are shown in Fig. 8 with heavy broken line for the comparison to the case of TRMM satellite only. The sampling error is about 5% through the latitudes and it is reduced by a factor of about two over the case of TRMM satellite observation only. Since the sampling error of one SSO satellite observation is about 6%, the combination of the TRMM and SSO satellites does not improve sampling error significantly over the case of one SSO satellite. This is because the sampling interval of the TRMM satellite differs from that of the SSO only about 30 min so that approximately half of observations during a month may be statistically redundant. Therefore, the actual number of independent sampling does not increase much.

4. Conclusion

A parameter study of satellite orbits was performed to estimate sampling errors of area-time averaged rain rates due to temporal sampling by satellite, especially for the low inclination satellites. The sampling characteristics were investigated by accounting for varying visiting intervals and varying fractions of averaging area on each visit as a function of the latitude of the grid box. Nomograms for sampling characteristics are presented for a range of orbital parameters centered at the nominal TRMM orbit. The sampling errors of area–time averaged rain rates were estimated by a simple model based on the observation that the lagged autocorrelation of area averaged rain rates decay exponentially with time. The variations of sampling intervals and sampling areas with orbital parameters and latitude were included in the model.

For the proposed TRMM satellite which will carry a passive microwave radiometer for direct measurement of precipitation, sampling errors would be about 10% of the monthly mean rain rate estimate over a 5° grid box. If we consider some uncertainties of parameters used, it might be more proper to say 8 to 12%. The effect of uneven sampling intervals with latitude tend to be offset by increasing sampling areas with latitude. Therefore, the latitude dependence of sampling error is not important. This error is almost equivalent to the sampling error produced by a sun-synchronous satellite whose altitude is about 700 km. This result illustrates that the TRMM satellite is much more effective for observing tropical precipitation than sun-synchronous satellites because of the small FOV provided by the low altitude orbit and the potential of removing expected diurnal cycle by the observation from the low inclination orbit.

Although no optimal weighting scheme was applied to integrate the data produced by two different satellites simultaneously, such system would be very effective on observing precipitation which is highly variable in space and time at least sampling error consideration. Well below the 10% of sampling error can be achieved by using two sunsynchronous satellites or one of them with the TRMM satellite. Probably the latter is more effective because of some advantages of the TRMM satellite on precipitation measurements.

The discussion has been based on sampling by a perfect instrument. But every instrument has its own inherent errors. The passive microwave radiometers for precipitation measurements also have calibration errors due to the limited information for some atmospheric and surface parameters. However, it is expected that individual contribution of these errors may be reduced by monthly averaging provided biases can be identified and removed. For example a significant source of bias would be the one due to beam-filling error.

The results presented provide a quantitative basis for estimating sampling error, insofar as the GATE rainfall statistics represent ITCZ conditions. We must be concerned about the uncertainties of some parameters in the model, especially for the extrapolated value of τ_0 and coefficient of variation on larger areas. The climatology of diurnal cycle should also be studied. We must be concerned about the representativeness of this model for conclusions about sampling errors to be expected in other parts of the tropics. The only way to answer this one is to use other approaches to estimate precipitation. One possibility is to use other satellite data such as GOES infrared cloud top temperatures to investigate the diurnal cycle, space-time lagged autocorrelation, etc. In this way one can assess the representativeness of GATE in so far as the present type of study applies throughout the tropics.

Acknowledgments. It is a pleasure to thank our colleagues David A. Short and Thomas L. Bell for their helpful discussions. We also acknowledge the support of NASA Headquarters through Grant GSFC 5-1503.

APPENDIX A

Equation of Orbital Motion of Satellite

The analyses introduced by Brooks (1977) are summarized. Among the forces exerted on orbiting satellites, the uneven gravitational force as a result of the earth's oblateness is the most important. For uniform

gravitational field, the unperturbed angular velocity of a satellite is

$$\Theta_0 = (\mu/r^3)^{1/2},$$

where μ is gravitational constant of the earth (398 601.2 $km^3\ s^{-2}$) and r is radius of satellite orbit ($a + h$, where a the mean radius of the earth and h the satellite altitude above surface). Following the first-order theory by Kozai (1959), involving the so-called J_2 term in the gravitational representation, the perturbed mean angular velocity of the satellite is

$$\Theta = \Theta_0\left[1 + \frac{3}{2} J_2 \frac{a^2}{r^2}\sqrt{1-\epsilon^2}\left(1 - \frac{3}{2}\sin^2 i\right)\right].$$

The dimensionless constant $\frac{3}{2} J_2$ is 1.6238235×10^{-3}, ϵ represents the eccentricity (=0 for circular orbit), and i is the inclination of satellite orbit. The angular velocity of precession on the orbital plane is then

$$\theta = \frac{3}{2} J_2 \frac{a^2}{r^2}\Theta(2 - 2.5\sin^2 i),$$

and that on the equator plane is

$$\omega = -\frac{3}{2} J_2 \frac{a^2}{r^2}\Theta \cos i.$$

The schematic of definitions of the orbital angles are illustrated below for circular orbit. Here τ_a denotes the anomalistic period, $\tau_a = 2\pi/\Theta$. Assume earth is not rotating. Due to the uneven gravitational force of the earth; a satellite around the earth will precess. Consider a sub-satellite point A (see Fig. 11) at the equator which a satellite passes at time t. After one anomalistic period τ_a, the satellite locates at a point A′ due to precession. (A′ is not over the equator.) Here, B is the sub-satellite point at the equator for the following rotation. Then the angle BOA′ is due to the precession on the orbital plane ($\theta \times \tau_a$) and the angle BOA is due to the precession on the equator plane ($\omega \times \tau_a$). Therefore total angular velocity on the orbital plane will be $\Theta + \theta$. For the rotating earth with angular velocity Ω, total angular velocity on the equator plane will be $\Omega - \omega$. (Note '−' sign on ω.)

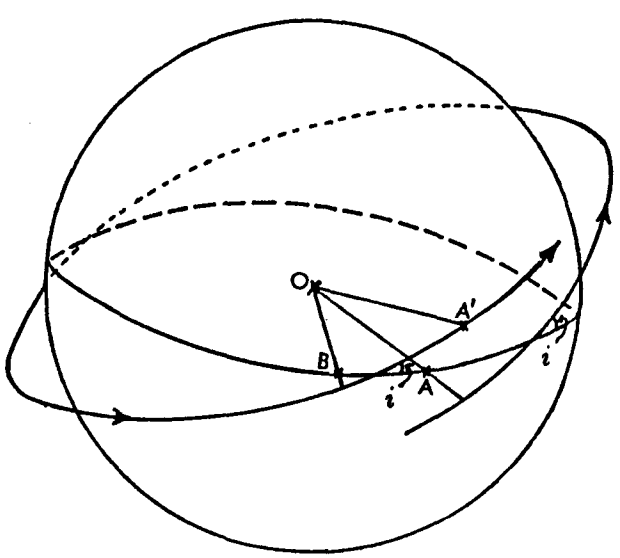

FIG. 11.

From these definitions with spherical geometry, Eqs. (1a) and (1b) can be derived. The higher order gravitational perturbation neglected here or some other sources of perturbation is less significant, these Eqs. provide an appreciation of the long term behavior of orbiting satellite at a level of complexity suitable for the initial phases of planning earth monitoring missions.

APPENDIX B

Derivation of Sampling Error

The sampling error is given by

$$\sigma_e^2 = E[(\hat{M}(T, t_0) - M(T))^2]$$
$$= E[M^2(T)] + E[\hat{M}^2(T, t_0)]$$
$$- 2E[\hat{M}(T, t_0)M(T)], \quad \text{(B1)}$$

where

$$E[M^2(T)] = E\left[\frac{1}{T^2}\int_{t_1}^{t_2} X(t)\mathrm{d}t \int_{t_1}^{t_2} X(s)\mathrm{d}s\right], \quad \text{(B2)}$$

$$E[\hat{M}^2(T, t_0)$$
$$= E\left[\frac{1}{N^2}\sum_{k=1}^{N} X(t + kt_0)\sum_{i=1}^{N} X(t + it_0)\right], \quad \text{(B3)}$$

and

$$E[\hat{M}(T, t_0)M(T)]$$
$$= E\left[\frac{1}{NT}\sum_{k=1}^{N} X(t + kt_0)\int_{t_1}^{t_2} X(t)\mathrm{d}t\right] \quad \text{(B4)}$$

with $T = t_2 - t_1$ and $Nt_0 = T$.

An assumption of ergodicity permits the evaluation of $E[Q]$ as the limit of a time average of Q, if the limit exists; that is

$$E[Q] = \lim_{L\to\infty}\frac{1}{L}\int_0^L Q(a)\mathrm{d}a$$

with L representing time. The true mean of $X(t)$, denoted by $\bar{X}$, may be calculated as

$$\bar{X} = \lim_{L\to\infty} \frac{1}{L}\int_0^L X(t)\mathrm{d}t.$$

The autocovariance function, $R(\tau)$, may be calculated as

$$R(\tau) = \lim_{L\to\infty} \frac{1}{L}\int_0^L (X(t) - \bar{X})(X(t+\tau) - \bar{X})\mathrm{d}t.$$

Upon expanding the terms in the intergrand, the following relationships are demonstratable.

$$R(\tau) = \lim_{L\to\infty} \frac{1}{L}\int_0^L X(t)X(t+\tau)\mathrm{d}t - \bar{X}^2.$$

With the assumption of the existence of $\bar{X}$ and $R(\tau)$, the expected values of each of the expressions in (B2), (B3), and (B4) are evaluated in turn.

$$E[M^2(T)] = \lim_{L\to\infty} \frac{1}{L}\int_0^L \left[\frac{1}{T^2}\int_0^T X(t+a)\mathrm{d}t \times \int_0^T X(s+a)\mathrm{d}s\right]\mathrm{d}a.$$

Upon interchanging the order of integration and letting $U = t + a$

$$E[M^2(T) = \frac{1}{T^2}\int_0^T\int_0^T \left[\lim_{L\to\infty}\frac{1}{L}\int_0^L X(U) \times X(U+s-t)\mathrm{d}U\right]\mathrm{d}s\mathrm{d}t$$

$$= \frac{1}{T^2}\int_0^T\int_0^T [R(s-t) + \bar{X}^2]\mathrm{d}s\mathrm{d}t.$$

This may be simplified further through inspection of the area in the s, t plane over which the integration is performed. $R(s-t)$ is constant along lines of the form $s = t + c$. These lines have a slope of 1 and an intercept of c. Choosing a coordinate system with one axis parallel to these lines simplifies evaluation of the integral, for R will be constant on all lines parallel to the axis. Letting $X = (s+t)/\sqrt{2}$, $y = (s-t)/\sqrt{2}$,

$$E[M^2(T)] = \frac{1}{T^2}\int_0^{T/\sqrt{2}}\int_{X=-\sqrt{2}T+y}^{X=\sqrt{2}T-y} [R(\sqrt{2}y) + \bar{X}^2]\mathrm{d}x\mathrm{d}y$$

and substituting $U = \sqrt{2}y$, after integration yields

$$E[M^2(T)] = \frac{2}{T}\int_0^T \left(1 - \frac{U}{T}\right)(R(U) + \bar{X}^2)\mathrm{d}U.$$

Reordering the sums in (B3) yields

$$E[\hat{M}^2(T, t_0)] = \lim_{L\to\infty}\frac{1}{L}\int_0^L \frac{1}{N^2} \times \sum_{k=1}^{N}\sum_{i=1}^{N} X(L+kt_0)X(L+it_0)\mathrm{d}L$$

and upon interchanging the order of integration and summation, letting $U = L + kt_0$,

$$E[\hat{M}^2(T, t_0)] = \frac{1}{N^2}\sum_{k=1}^{N}\sum_{i=1}^{N}(R(i-k)t_0) + \bar{X}^2.$$

Evaluation of the double sum using the relationship $R(\tau) = R(-\tau)$ yields

$$E[\hat{M}^2(T, t_0)] = \frac{R(0)}{N} + \frac{2}{N}\sum_{j=1}^{N-1}\left(1 - \frac{j}{N}\right)(R(jt_0) + \bar{X}^2). \quad \text{(B6)}$$

Equation (B4) may be evaluated with the same techniques as used in evaluation of (B2) and (B3).

$$E[\hat{M}(T, t_0)M(T)] = \frac{1}{NT}\sum_{k=1}^{N}\int_0^T (R(t - kt_0) + \bar{X}^2)\mathrm{d}t. \quad \text{(B7)}$$

Substitution of (B5), (B6), and (B7) into (B1) yields

$$\sigma_e^2 = \frac{2}{T}\int_0^T\left(1 - \frac{\tau}{T}\right)R(\tau)\mathrm{d}\tau + \frac{R(0)}{N} + \frac{2}{N}\sum_{k=1}^{N-1}\left(1 - \frac{k}{N}\right)R(kt_0) - \frac{2}{NT}\sum_{k=1}^{N}\int_0^T R(\tau - kt_0)\mathrm{d}\tau. \quad \text{(B8)}$$

The sampling error for an exponential autocovariance function of the form $R(\tau) = Be^{-|\tau|/\tau_0}$ can be calculated by the substitution to (B8), and using the relationship

$$\sum_{j=1}^{N} A^j = \frac{A(1-A^N)}{(1-A)}.$$

After some arrangements,

$$\sigma_e^2 = \frac{2B}{(T/\tau_0)}\left[-1 + \frac{t_0}{2\tau_0}\left(\frac{e^{t_0/\tau_0}+1}{e^{t_0/\tau_0}-1}\right) + \frac{e^{-T/\tau_0}-1}{(T/\tau_0)}\left\{1 - \frac{t_0}{\tau_0}\left(\frac{e^{t_0/\tau_0}+1}{e^{t_0/\tau_0}-1}\right) + \left(\frac{t_0}{\tau_0}\right)^2\frac{e^{t_0/\tau_0}}{(e^{t_0/\tau_0}-1)^2}\right\}\right]. \quad \text{(B9)}$$

REFERENCES

Albright, M. D., D. R. Mock, E. E. Recker and R. J. Reed, 1981: A diagnostic study of the diurnal rainfall variation in the GATE B-scale area. *J. Atmos. Sci.*, **38,** 1429–1445.

——, E. E. Recker, R. J. Reed and R. Dang, 1985: The diurnal variation of deep convection and infrared precipitation in the central tropical pacific during January–February 1979. *Mon. Wea. Rev.*, **113,** 1663–1680.

Arkin, P., 1979: The relationship between fractional coverage of high cloud and rainfall accumulations during GATE over the B-scale array. *Mon. Wea. Rev.*, **107,** 1382–1387.

Barret, E. C., and D. W. Martin, 1981: *The use of satellite data in rainfall monitoring.* Academic Press, 340 pp.

Bell, T. L., 1987: A space-time stochastic model of rainfall for satellite remote-sensing studies. *J. Geophys. Res.*, **92,** 9631–9643.

Brooks, D. R., 1977: An introduction to orbit dynamics and its application to satellite based earth monitoring missions. NASA Ref. Publication 1009 Washington, DC, 80 pp. [NTIS No. N78-12113]

Kedem, B., L. Chiu and G. North, 1987: Estimation of mean rain rate: Application to satellite observation. *J. Geophys. Res.*, (submitted).

Hudlow, M. D., and V. L. Patterson, 1979: *GATE Radar Rainfall Atlas.* NOAA Special Report, available from U.S. Govt. Printing Office, Wash., DC 20402, 158 pp. [NTIS No. N80-21003]

Kozai, Y., 1959: The motion of a close earth satellite. *Astron. J.*, **64,** 367–377.

Laughlin, C. R., 1981: On the effect of temporal sampling on the observation of mean rainfall. *Precipitation Measurements from Space,* Atlas D. & O. Thiele, editors, available from NASA/GSFC, Greenbelt, MD, 20771.

McConnell, A., and G. North, 1987: Sampling errors in satellite estimates of tropical rain. *J. Geophys. Res.*, **92,** 9567–9570.

North, G. R., 1987: Sampling studies for satellite estimation of rain, *Preprints 10th Conf. on Probability and Statistics in Atmospheric Science, Edmonton,* Amer. Meteor. Soc., 129–135.

Reed, R. J., and K. D. Jaffe, 1981: Diurnal variation of summer convection over West Africa and the tropical eastern Atlantic during 1974 and 1978. *Mon. Wea. Rev.*, **109,** 2527–2534.

Simpson, J. R., R. Adler and G. North, 1988: A proposed tropical rainfall measuring mission (TRMM) satellite. *Bull. Amer. Meteor. Soc.*, **69,** 278–295.

Thiele, O. W., 1987: On requirements for a satellite mission to measure tropical rainfall. NASA Ref. Publication 1183, Washington, DC, 49 pp. [NTIS No. N87-20701]

Wilheit, T. T., 1986: Some comments on passive microwave measurement of rain. *Bull. Amer. Meteor. Soc.*, **67,** 1226–1232.